# High Sensitivity Temperature Sensor Based on Harmonic Vernier Effect

Meifang HE, Beibei ZHU, and Zuxing ZHANG*

*Advanced Photonic Technology Lab, College of Electronic and Optical Engineering, Nanjing University of Posts and Telecommunications, Nanjing 210023, China*

*Corresponding author: Zuxing ZHANG E-mail: zxzhang@njupt.edu.cn

**Abstract:** A high-sensitivity temperature sensor based on the harmonic Vernier effect is proposed and verified by experiments. The main component of the sensor is a Sagnac interferometer consisting of two sections of polarization maintaining fibers (PMFs) spliced with an intersection angle of 45° between their fast axes. The harmonic Vernier effect is achieved by setting the length of one of the PMFs an integral multiple (*i*-times) of the length of the other plus a detuning factor. Compared with the Sagnac interferometer based on the fundamental Vernier effect, the temperature sensitivity of the harmonic Vernier effect is higher, reaching *i*+1 times of that of the fundamental Vernier effect (*i* is the order of the harmonic).

**Keywords:** Harmonic Vernier; temperature sensor; polarization maintaining fiber; Sagnac interferometer

Citation: Meifang HE, Beibei ZHU, and Zuxing ZHANG, "High Sensitivity Temperature Sensor Based on Harmonic Vernier Effect," *Photonic Sensors*, 2023, 13(2): 230204.

## 1. Introduction

Optical fiber sensors have the advantages of corrosion resistance, electromagnetic interference resistance, and small size. They are widely used in temperature, strain, pressure, magnetic field, humidity, and other sensing fields [1–5]. In order to improve the performance of optical fiber sensors, researchers have conducted a lot of research on the structure and materials of optical fiber sensors [6–10].

Recently, researchers have further improved the sensitivity of sensors by applying the optical Vernier effect [11–14]. For example, Shao *et al*. [15] proposed a temperature sensor based on cascaded two Sagnac interferometers (SIs) and the sensitivity reached –13.36 nm/℃, which was 9 times higher than that of a single SI. Yang *et al*. [16] reported a temperature sensor cascaded by Fabry-Perot interferometer (FPI) and SI, and the Vernier effect increased the sensitivity to 29 nm/℃ by nearly 20 times. However, the above two structures are relatively complex, and two Sagnac rings need to be cascaded to achieve the Vernier amplification effect. Then, Zhao *et al.* [17] proposed a temperature sensor based on the fundamental Vernier effect, through embedding two sections of the polarization maintaining fiber (PMF) with small length difference into a Sagnac ring. The sensitivity reached 2.44 nm/℃, which was 14.97 times higher than that of the temperature sensor with ordinary Sagnac interference. But the sensing sensitivity of this structure is still not high enough to measure weak temperature changes. Fortunately, Gomes *et al.* [18] proposed the concept of the optical harmonic Vernier effect and verified that the amplification ability of harmonic Vernier increased with an increase in the harmonic order. And Chen *et al.* [19]

Received: 22 July 2022 / Revised: 02 December 2022

DOI: 10.1007/s13320-023-0677-x
Article type: Regular

proposed that, without reference envelope modulation, the transition from Vernier effect to harmonic Vernier effect could be achieved through spectrum envelope modulation caused by photon coupling in coupled resonators. This method provides a new idea for the realization of harmonic Vernier.

In this paper, we propose a high-sensitivity temperature sensor based on the harmonic Vernier effect. The structure of the sensor is a Sagnac interferometer consisting of two sections of PMFs (PMF-SI) spliced with an intersection angle of 45° between their fast axes. The harmonic Vernier effect is achieved by setting the length of one of the PMFs an integral multiple ($i$-times) of the length of the other plus a detuning factor ($\Delta$). In order to improve the sensitivity of the sensor, the effects of the harmonic order and the detuning on the sensitivity of sensor are discussed theoretically and experimentally. And when the detuning is 2.5 cm, the PMF-SI based on the second-order Vernier effect has reached a high sensitivity of –40.73 nm/℃ in a small range of temperature fluctuations. Compared with the cascaded SIs temperature sensor, the PMF-SI based on the second-order Vernier effect proposed by us has the advantages of simple manufacturing, low insertion loss, and high temperature sensitivity, and has potential applications in high-precision temperature measurement fields such as medicine, biology, and chemistry.

## 2. Theory and analysis

Figure 1 is the schematic diagram of PMF-SI, which is composed of a 3 dB coupler and two sections of PMFs (PM 1550-XP). The birefringence coefficient of the PMF is linearly related to temperature within a certain temperature range and is greatly affected by temperature, so it can be used for temperature sensing. The two sections of PMFs are spliced with an intersection angle of 45° between their fast axes by the polarization maintaining fusion splicer, and $\theta$ is the welding angle in Fig. 1. The other end of the PMF is welded with the single-mode fiber of the coupler.

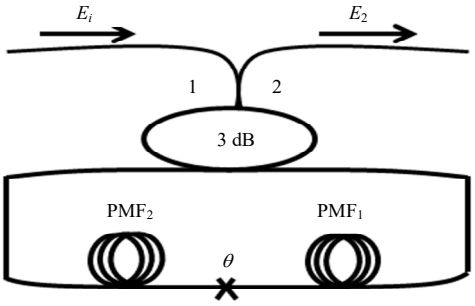


Fig. 1 Experimental schematic diagram.

As shown in Fig. 1, the 3 dB coupler divides the input light $E_i$ into two paths of light transmitted clockwise and counterclockwise along the Sagnac ring. After the two paths of light are transmitted around the Sagnac ring, they interfere at the coupler. The transmission spectrum $E_2$ of the interference light can be measured by an optical spectrum analyzer [20]. Let the length of the sensing optical fiber $PMF_1$ be $L_1$ and the length of the reference optical fiber $PMF_2$ be $L_2$. According to Jones matrix analysis, the clockwise transmission matrix $\mathbf{J}_1$ of two polarization maintaining fibers embedded in a Sagnac ring is the result of left multiplication of the Jones matrix of $PMF_2$, the $\theta$ and $PMF_1$. So $\mathbf{J}_1$ is

$$\mathbf{J}_1 = \mathbf{J}_{\mathrm{PMF}_2}\mathbf{R}(\theta)\mathbf{J}_{\mathrm{PMF}_1} = \begin{bmatrix} \mathrm{e}^{-\mathrm{j}\varphi_2} & 0 \\ 0 & \mathrm{e}^{\mathrm{j}\varphi_2} \end{bmatrix}\begin{bmatrix} \cos\theta & \sin\theta \\ -\sin\theta & \cos\theta \end{bmatrix}\begin{bmatrix} \mathrm{e}^{-\mathrm{j}\varphi_1} & 0 \\ 0 & \mathrm{e}^{\mathrm{j}\varphi_1} \end{bmatrix} \quad (1)$$

where $\varphi_1$ and $\varphi_2$ are the phase differences generated by light passing through $PMF_1$ and $PMF_2$ respectively, which are proportional to the length and the birefringence coefficient of the PMF [21, 22]. And the birefringence coefficient of the PMF we used is $3.5\times10^{-4}$ at room temperature. Similarly, the counterclockwise transmission matrix $\mathbf{J}_2$ in the Sagnac ring is the result of left multiplication of Jones matrix of $PMF_1$, $\theta$, and $PMF_2$. So $\mathbf{J}_2$ is

$$\mathbf{J}_2 = \mathbf{J}_{\mathrm{PMF}_1}\mathbf{R}(\theta)\mathbf{J}_{\mathrm{PMF}_2} = \begin{bmatrix} \mathrm{e}^{-\mathrm{j}\varphi_1} & 0 \\ 0 & \mathrm{e}^{\mathrm{j}\varphi_1} \end{bmatrix}\begin{bmatrix} \cos\theta & \sin\theta \\ -\sin\theta & \cos\theta \end{bmatrix}\begin{bmatrix} \mathrm{e}^{-\mathrm{j}\varphi_2} & 0 \\ 0 & \mathrm{e}^{\mathrm{j}\varphi_2} \end{bmatrix}. \quad (2)$$

According to the Jones matrix of the 3 dB coupler, we can deduce the expressions of reflected light $E_1$ and transmitted light $E_2$ output by the coupler. $E_1$ and $E_2$ can be expressed as

$$\begin{aligned} E_1 &= \mathrm{j}\left(\mathbf{J}_1 + \mathbf{J}_2\right) E_i / 2 \\ E_2 &= \left(\mathbf{J}_1 - \mathbf{J}_2\right) E_i / 2. \end{aligned} \tag{3}$$

Therefore, the transmission formula of the PMF-SI is

$$\begin{aligned} T &= \frac{E_2^{\ 2}}{E_i^2} \\ &= \left[\cos\left(\varphi_1 + \varphi_2\right)\cos\theta + \cos\left(\varphi_1 - \cos\varphi_2\right)\sin\theta\right]^2. \end{aligned} \tag{4}$$

The next thing is to verify the relationship between the Vernier effect of the PMF-SI and $\theta$ by simulation. Let $L_1$ be 40 cm and $L_2$ be 37.5 cm, and change the value of $\theta$. The simulation results are shown in Fig. 2.

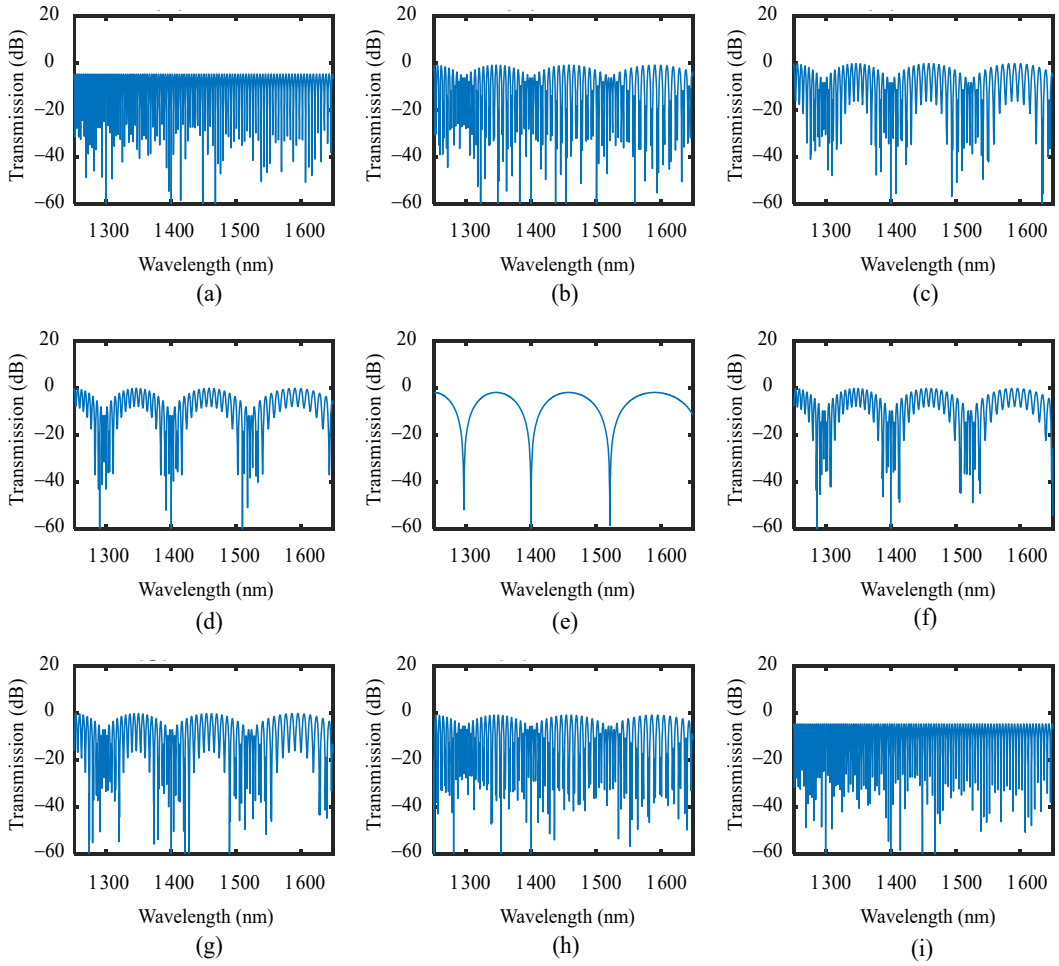


Fig. 2 Simulation results of transmission spectra changing with the intersection angle: (a) $\theta$=0°, (b) $\theta$=30°, (c) $\theta$=45°, (d) $\theta$=60°, (e) $\theta$=90°, (f) $\theta$=120°, (g) $\theta$=135°, (h) $\theta$=150°, and (i) $\theta$=180°.

It can be seen from the simulation results that the Vernier effect is very obvious when $\theta$ is 45° or 135°. Thus, in this paper, the Vernier effect of the interferometer is investigated when $\theta$ is set to 45°.

After $\theta$ is set to 45°, the influence of the length of PMFs on the Vernier effect of the PMF-SI is further discussed. Let $L_1$ remain unchanged and $L_2$ be

$$L_2^i = (i+1)L_1 - \Delta \tag{5}$$

where $i$ is the order of harmonics and $\Delta$ is the amount of detuning. When $i$=0, the condition of the fundamental Vernier is satisfied for $L_1$ and $L_2$; when $i$ is a positive integer greater than 0, the condition of the harmonic Vernier is satisfied for $L_1$ and $L_2$. To verify this assumption, let $L_1$ be 40 cm, $L_2$ be 37.5 cm, 77.5 cm, and 117.5 cm in turn, that is, let $i$ be 0, 1,

and 2 in turn and keep $\Delta$ as 2.5 cm. And the simulation results are shown in the Fig. 3.

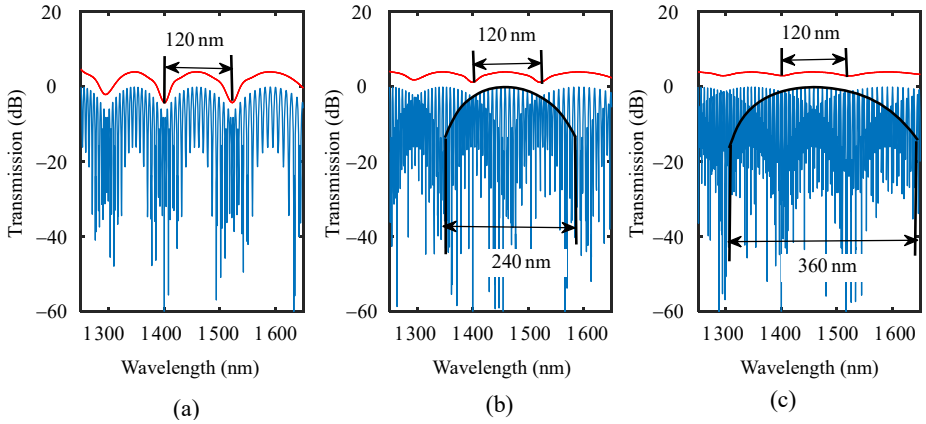


Fig. 3 Simulated transmission spectra of the PMF-SI with different harmonic order $i$: (a) fundamental Vernier, $i$=0, (b) first harmonic, $i$=1, and (c) to second harmonic, $i$=2. (Red line: the upper envelope of the interference spectrum; black line: part of the inner envelope of the interference spectrum).

It can be seen from Fig. 3 that the interference spectrum changes from the fundamental Vernier to the harmonic Vernier with an increase in $i$ when $L_1$ and $L_2$ are satisfied with (5).

$FSR_{enevlope}$, the free spectral range of the upper envelope of the interference spectrum, is determined by $FSR_1$ and $FSR_2$ ($FSR_1$ and $FSR_2$ are the free spectral ranges of SIs with the single section of $PMF_1$ and $PMF_2$, respectively). It can be seen from Fig. 3 that the FSR of the upper envelope of the harmonic Vernier effect is the same as that of the fundamental Vernier effect, but the contrast of the upper envelope of the harmonic Vernier is getting lower and lower with harmonic order increase. In addition, it also confirms that the free spectral range of the inner envelope of the interference spectrum $FSR_{interenevlope}$ is $i$+1 times of $FSR_{enevlope}$. In practical applications, we usually monitor the wavelength shift of the high-order harmonic envelope to obtain higher sensing sensitivity. Since the contrast of the upper envelope of the high-order harmonic is low, we use the inner envelope of the harmonic Vernier effect to replace the upper envelope of it, and the intersection of the inner envelope is used as the reference point to monitor the wavelength shift of the transmission spectrum.

To verify the relationship between $FSR_{interenevlope}$ and $\Delta$, let $L_1$ be 50 cm, $L_2$ be 97 cm, 96 cm, and 94 cm in turn, that is, $\Delta$ is 3 cm, 4 cm, and 5 cm, respectively. The simulation results are shown in Fig. 4.

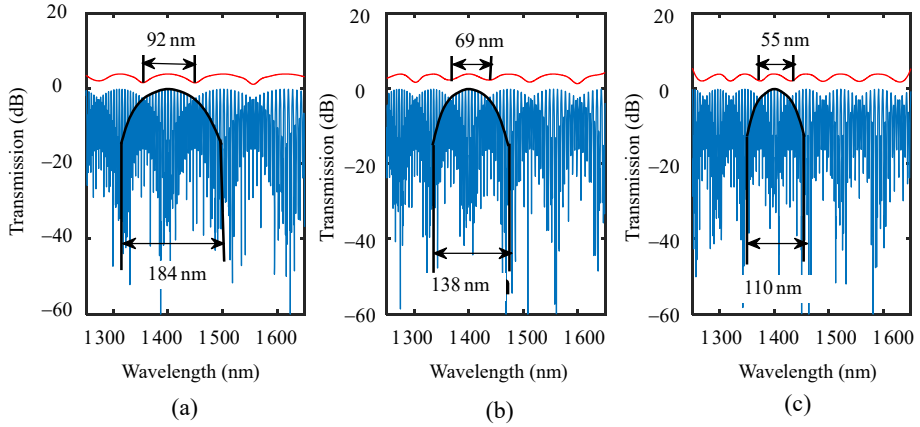


Fig. 4 Simulation results of the evolution of the transmission spectra of the interferometer with different values of $\Delta$: (a) $\Delta$=3, (b) $\Delta$=4, and (c) $\Delta$=5. (Red line: the upper envelope of the interference spectrum; black line: part of the inner envelope of the interference spectrum).

It can be seen that $FSR_{interenevlope}$ is inversely proportional to $\Delta$ in Fig. 4. Another important parameter of the Vernier effect is the magnification factor ($M$). For the fundamental Vernier effect, $M_0$ is defined as the ratio of FSR of the upper envelope to $FSR_1$ [17]. So $M$ is

$$M_0 = \frac{FSR_{enevlope}}{FSR_1} = \frac{L_1}{|\Delta|}. \tag{6}$$

For the harmonic Vernier effect, $M^i$ is defined as the ratio of FSR of the inner envelope to $FSR_1$ [17]. So $M^i$ is

$$M^i = \frac{FSR^i_{int\,erenevlope}}{FSR_1} = (i+1)M_0. \tag{7}$$

It can be seen from (6) and (7) that the sensing sensitivity of the harmonic Vernier is $i$+1 times that of the fundamental Vernier, and the sensitivity increases with an increase in the harmonic order, and decreases with an increase in $\Delta$.

## 3. Experiments and results

The experimental setup is shown in Fig. 5. A broadband light source (BBS) with a wavelength range of 1 250 nm to 1 650 nm is used to provide incident light which is input from Port 1 of a 3 dB coupler. The reference optical fiber $PMF_2$ is placed at room temperature. The sensing fiber $PMF_1$ is then partially heated by a column oven with an accuracy of 0.1 ℃. And the heated length of $PMF_1$ is only 31 cm due to the limitation of the length of the column oven. In order to avoid the influence of stress on the experiment, the PMFs are always in a straight state by the clamp. At last, the transmission spectrum from Port 2 of the coupler is measured by an optical spectrum analyzer (OSA).

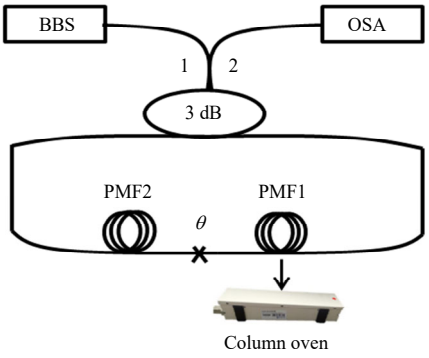


Fig. 5 Experimental setup diagram.

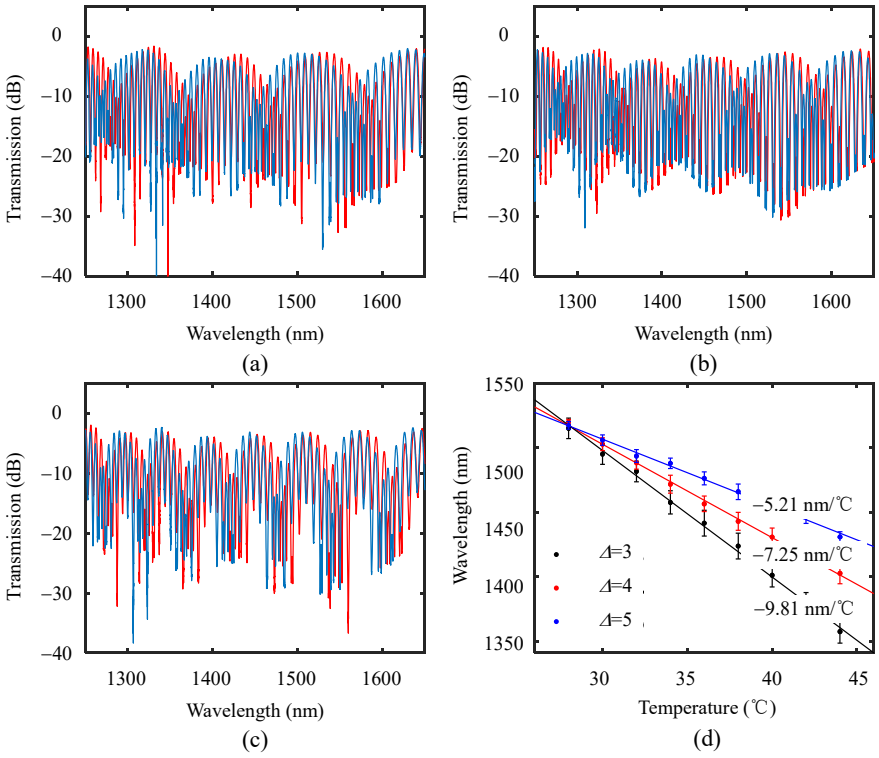


Fig. 6 Transmission spectra with different values of $\Delta$: (a) $\Delta$=3 cm, (b) $\Delta$=4 cm, and (c) $\Delta$=5 cm (Red line: transmission spectra at 30 ℃; blue line: transmission spectra at 32 ℃); (d) temperature sensitivity corresponding to different detuning.

The length of $PMF_1$ is 66 cm and the length of $PMF_2$ is chosen to be 63 cm, 62 cm, and 61 cm, respectively, that is, $\Delta$ is 3 cm, 4 cm, and 5 cm, respectively. The heating range of the oven is set from 28 °C to 44 °C in a 2 °C step. The experimental results are shown in Fig. 6. Figures 6(a)–6(c) are the transmission spectra of different $\Delta$ at 30 °C and 32 °C, respectively. It can be seen that the spectrum appears blue-shifted when the temperature is increased. Figure 6(d) is the transformation relationship of wavelength offset with temperature. As shown in Fig. 6(d), when $\Delta$ is 3 cm, 4 cm, and 5 cm, the corresponding temperature sensitivities of PMF-SI are –9.81 nm/°C, –7.25 nm/°C, and –5.21 nm/°C. Therefore, it can be calculated that the temperature sensitivity of the PMF-SI is inversely proportional to $\Delta$.

Then, the length of $PMF_1$ is 40 cm, and the length of $PMF_2$ is selected to be 37.5 cm, 77.5 cm, and 117.5 cm respectively, that is, $\Delta$ is kept as 2.5 cm unchanged, and the order of harmonics is varying. The heating range of the oven is set from 29 °C to 36 °C with a step size of 1 °C. The experimental results are shown in Fig. 7. Figures 7(a)–7(c) represent the transmission spectra of the PMF-SI when $i$ is 0, 1, and 2 in turn, and Fig. 7(d) represents the temperature sensitivity. As shown in Fig. 7(d), when $i$ is 0, 1, and 2, the corresponding temperature sensitivities of PMF-SI are –13.54 nm/°C, –25.97 nm/°C, and –40.73 nm/°C. And the ratios of the temperature sensitivity of the first two harmonic orders to that of the fundamental Vernier effect are 1.92 and 3.02, respectively. The experimental results prove that the temperature sensitivity of the PMF-SI based on the harmonic Vernier effect is $i$+1 times that of the PMF-SI based on the fundamental Vernier effect.

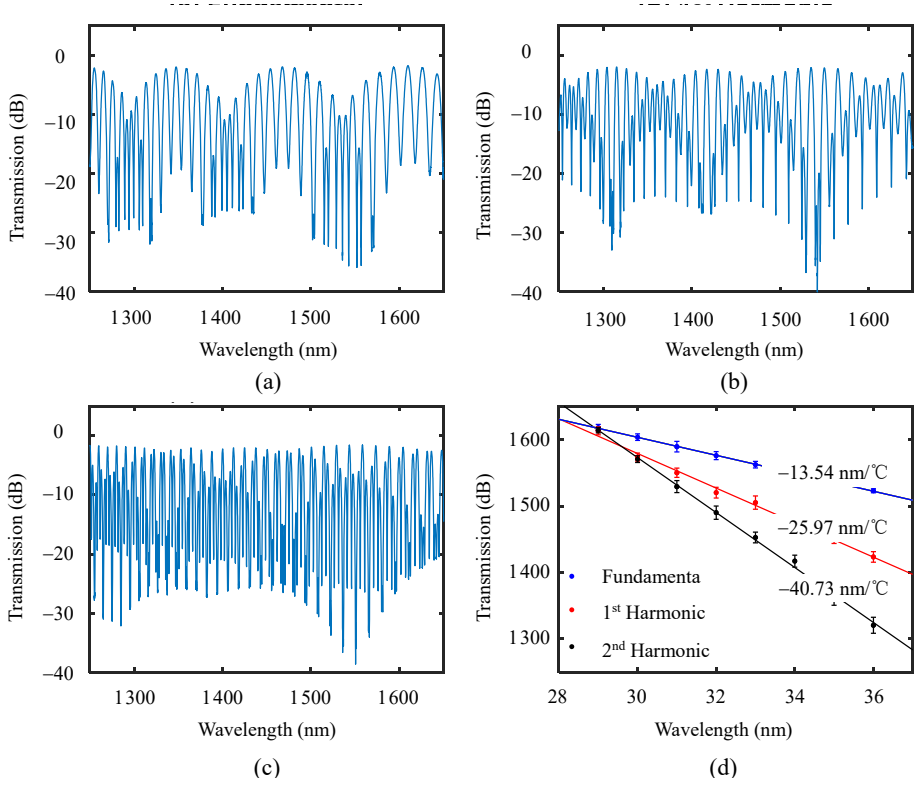


Fig. 7 Transmission spectra of (a) fundamental Vernier effect, (b) first-order Vernier effect, and (c) second-order Vernier effect, respectively; (d) corresponding temperature sensitivity.

## 4. Conclusions

In this paper, we propose a PMF-SI temperature sensor based on the harmonic Vernier effect. The structure of the PMF-SI is that two sections of PMFs with lengths of a multiple relationship plus detuning

factor are spliced with an intersection angle of 45° between their fast axes. The harmonic Vernier effect is realized in this structure to enhance the temperature sensitivity of the PMF-SI. It is proved by theory and simulation that the temperature sensing sensitivity of the PMF-SI is inversely proportional to $\Delta$, and it is confirmed that the amplification effect of the harmonic Vernier effect is $i$+1 times that of the fundamental Vernier effect Theoretically, the order of harmonics can be infinitely increased, and the sensitivity of the corresponding sensor can also be infinitely increased. But experimentally, as the modulation contrast of the upper envelope decreases with an increase in the harmonic order, the visibility of modulation will be deteriorated due to signal noise. So the order of harmonics can't be infinitely increased in the experiment. In addition, limited by the wavelength range of BBS and the monitoring range of OSA used in the experiment, the measurable temperature range of the sensor will decrease with an increase in the sensor sensitivity. Considering the sensitivity and measurable temperature range of the sensor, we finally propose a PMF-SI temperature sensor with a detuning of 2.5 cm based on the second-order Vernier effect, which can achieve the optimum sensitivity in the temperature range of our experiment.

The experimental results show that the temperature sensitivity of the PMF-SI based on the second-order Vernier effect can reach –40.73 nm/°C, which is 3.02 times that of the PMF-SI based on the fundamental Vernier effect. The proposed PMF-SI based on the harmonic Vernier effect has the advantages of simple structure, low cost, and high sensing sensitivity, which is especially sensitive to weak temperature changes. It has broad application prospects for accurate temperature sensing.

## Acknowledgment

We acknowledge the supports from the National Natural Science Foundation of China (Grant No. 62175116) and 1311 Talent Plan of Nanjing University of Posts and Telecommunications.



## References

[1] Y. X. Jiang, Y. T. Yi, G. Brambilla, and P. F. Wang, "Ultra-high-sensitivity refractive index sensor based on dual-microfiber coupler structure with the Vernier effect," *Optics Letters*, 2020, 45(5): 1268–1271.

[2] P. M. R. Robalinho, A. D. Gomes, and O. Frazao, "High enhancement strain sensor based on Vernier effect using 2-fiber loop mirrors," *IEEE Photonics Technology Letters*, 2020, 32(18): 1139–1142.

[3] W. Q. Feng, Z. Y. Liu, H. Y. Tam, and J. H. Yin, "The pore water pressure sensor based on Sagnac interferometer with polarization-maintaining photonic crystal fiber for the geotechnical engineering," *Measurement*, 2016, 90: 208–214.

[4] F. F. Wei, A. K. Mallik, D. J. Liu, Q. Wu, G. D. Peng, G. Farrell, *et al*., "Magnetic field sensor based on a combination of a microfiber coupler covered with magnetic fluid and a Sagnac loop," *Scientific Reports*, 2017, 7(1): 4725.

[5] L. P. Sun, J. Li, L. Jin, Y. Ran, and B. O. Guan, "High-birefringence microfiber Sagnac interferometer based humidity sensor," *Sensors and Actuators B*: *Chemical*, 2016, 231: 696–700.

[6] R. Zeltner, R. Pennetta, S. R. Xie, and P. S. J. Russell, "Flying particle microlaser and temperature sensor in hollow-core photonic crystal fiber," *Optics Letters*, 2018, 43(7): 1479–1482.

[7] H. L. Wang and A. J. Yang, "Temperature sensing property of hollow-core photonic bandgap fiber filled with CdSe/ZnS quantum dots in an UV curing adhesive," *Optical Fiber Technology*, 2017, 38: 104–107.

[8] B. Feng, Y. Liu, and S. L. Qu, "High-temperature sensor based on resonant reflection in hollow core fiber," *Optical Engineering*, 2016, 55(10): 106127.

[9] L. V. Nguyen, D. Hwang, S. Moon, D. S. Moon, and Y. Chung, "High temperature fiber sensor with high sensitivity based on core diameter mismatch," *Optics Express*, 2008, 16(15): 11369–11375.

[10] C. T. Wang, C. Y. Wang, J. H. Yu, L. T. Kuo, C. W. Tseng, H. C. Jau, *et al.*, "Highly sensitive optical temperature sensor based on a SiN micro-ring resonator with liquid crystal cladding," *Optics*

*Express*, 2016, 24(2): 1002–1007.

[11] L. G. Abbas, "Vernier effect based strain sensor with cascaded Fabry-Perot interferometers," *IEEE Sensors Journal*, 2020, 20(16): 9196–9201.

[12] H. Gao, J. Wang, J. Shen, D. Xu, Y. Zhang, and C. Li, "Study of the Vernier effect based on the Fabry-Perot interferometer: methodology and application," *Photonics*, 2021, 8(8): 304.

[13] G. M. Zuo, L.Xia, J. Chen, Z. Yang, and Y. Wu, "The order calibration of Vernier squared envelope extracted by the Hilbert-Huang transform," *Journal of Lightwave Technology*, 2020, 39(6): 1880–1886.

[14] X. H. Fang, W. Zhang, J. W. Li, C. L. Lin, Z. Chen, M. Zhang, *et al*., "Signal processing assisted Vernier effect in a single interferometer for sensitivity magnification," *Optics Express*, 2021, 29(8): 11570–11581.

[15] L. Y. Shao, Y. Luo, Z. Y. Zhang, X. H. Zou, B. Luo, W. Pan, *et al.*, "Sensitivity-enhanced temperature sensor with cascaded fiber optic Sagnac interferometers based on Vernier-effect," *Optics Communications*, 2015, 336: 73–76.

[16] Y. Q. Yang, Y. G. Wang, Y. X. Zhao, and J. X. Jiang, "Sensitivity-enhanced temperature sensor by hybrid cascaded configuration of a Sagnac loop and a F-P cavity," *Optics Express*, 2017, 25(26): 33290–33296.

[17] Q. L. Zhao, Z. M. Ding, B. Q. Wu, "Vernier effect based on optical fiber Sagnac interference loop with two angle shift spliced polarization maintaining fibers and its application on temperature sensor," *Optics and Precision Engineering*, 2017, 25(9): 2283–2291.

[18] A. D. Gomes, M. S. Ferreira, J. Bierlich, J. Kobelke, M. Rothhardt, H. Bartelt, *et al.*, "Optical harmonic vernier effect: a new tool for high performance interferometric fibre sensors," *Sensors*, 2019, 19(24): 5431.

[19] L. Chen, J. H. Huang, G. S. Liu, F. F. Huang, H. Zheng, Y. Chen, *et al.*, "Photon coupling-induced spectrum envelope modulation in the coupled resonators from Vernier effect to harmonic Vernier effect," *Nanophotonics*, 2022, 11(5): 957–966.

[20] Z. L. Ran, X. He, Y. J. Rao, D. Sun, X. J. Qin, D. B. Zeng, *et al.*, "Fiber-optic microstructure sensors: a review," *Photonic Sensors*, 2021, 11(2): 227–261.

[21] J. Shi, Y. Y. Wang, D. G. Xu, H. W. Zhang, G. Su, L. Duan, *et al.*, "Temperature sensor based on fiber ring laser with Sagnac loop," *IEEE Photonics Technology Letters*, 2016, 28(7):794–797.

[22] L. P. Shao, J. H. Hu, H. L. Lu, J. Du, T. Y. Wu, and Y. P. Wang, "High-sensitivity temperature sensor based on polarization maintaining fiber Sagnac loop," *Photonic Sensors*, 2019, 9(1): 25–32.